Effect of Micromechanical Models on Mechanical Behavior of Functionally Graded Plates Based on a Quasi-3D Hyperbolic Shear Deformation Theory

Hong-Yan Chen

School of Mechanical Engineering, University of Science and Technology Beijing, Beijing 10083, China.
Shunde Graduate School, University of Science and Technology Beijing, Foshan 528300, China.

Wei Li

School of Applied Science, Beijing Information Science and Technology University, Beijing, 100192, China.
E-mail: webbli @163.com

Jun-Ning Zhang

Shanghai Key Laboratory of Mechanics in Energy Engineering, Shanghai Institute of Applied Mathematics and Mechanics, School of Mechanics and Engineering Science, Shanghai University, Shanghai, 200444, China.

(Received 22 November 2023; accepted 10 March 2024)

Five alternative micromechanical models (Voigt, Reuss, Tamura, LRVE, Hashin) are used to predict the valid material properties of a simply-supported functionally graded materials (FGM) plate. The free vibration and static behavior are studied based on a quasi-3D hyperbolic shear deformation theory considering the stretching effect. The profile of an FGM plate is assumed by the power-law, Sigmoid and exponential functions. The numerical results of an FGM plate behavior reveal via Navier-type solution. The temperature effects of the micromechanical models on the fundamental frequency and transverse displacement for an FGM plate are also discussed. By analyzing the influence of different micro-models on the mechanical behavior of an FGM plate, researchers can objectively understand the establishment and differences of structural micromechanical models. And considering the actual high temperature situation, the deformation prediction ability of the structure is predicted. This study provides theoretical guidance for the analysis and modeling of FGM structures for the purpose of engineering practice.

1. INTRODUCTION

FGMs are made up of two or more kinds of media in the micro fusion[1–4] with no obvious phase interface. Compared with other composite materials, FGMs have many advantages, such as meeting special work environment requirements by adjusting the volume fraction and the distribution type, having high specific strength and stiffness, etc.. The FGM plate has been widely used in construction, aerospace, high-speed rail, civil engineering and other fields.[5–8] Because of the heterogeneity along the thickness direction of the composite structure, the mechanical properties of the structure will be much more complicated. Therefore, it is very important to test the effect of an alternative micromechanical model on the mechanical behavior of FGM structures.

To describe the effective properties of an FGM plate accurately, a diversity of micromechanical models are discussed in the literature. For example, Gasik[9] outlined the efficient modelling approaches of FGMs to provide accurate estimates of the properties. Rahman et al.[10] presented a stochastic micromechanical model to predict probabilistic characteristics of elastic mechanical properties of an isotropic structure. Yin et al.[11] studied the thermoelastic behavior of functionally graded particulate materials using a micromechanical approach. A micromechanical model, used to determine the effective thermal conductivity, and thermal expansion coefficient is presented for predicting the effective thermo-viscoelastic behavior of an FGM.[12] Akbarzadeh et al.[13] examined the influence of micromechanical models on the macroscopic behavior of a functionally graded plate based on classical and shear-deformation plate theories. However, a few of the standard micromechanical models should be specifically mentioned[14–19] Voigt[14,19] and Reuss[15] used the simplest model to evaluate the material properties of composites effectively. Hashin[16] found the improved upper and lower bounds of heterogeneous materials successfully by using the variational principle. Tamura et al.[17] proposed a linear rule of mixture for effective properties with an empirical fitting parameter. Gasik and Lilius[18] employed the cubic local representative volume elements (LRVE) to show the effective material properties. The development of these types of models has improved the modeling theory and has been recognized by researchers.

In addition, accurate and high efficiency displacement fields are crucial to accurately predict mechanical behavior. Hence, many theories have been put forward successively. First, the classical laminated plate theory (CLPT) was developed. However it neglects the influence of the transverse shearing deformation.[20,21] Then, the first-order shear deformation theory (FSDT)[22–24] appeared. It is directly dependent on the reason-

able shear correction factor. Later, different higher-order shear deformation plate theories (HSDT) depending on the transverse shear deformation function subsequently appeared. The constraint of the shear correction factor is not required.[25–29] In engineering, the tendency is to produce transverse stretching in the process of deformation for thick plates or shells, so it should not ignore the stretching effects along the thickness direction. As a result, Li et al.[30] proposed a displacement field with transverse stretching effects, which can be expanded into Chebyshev series multiplying by a function. Carrera et al.[31] verified the transverse stretching on the transverse normal stress distribution of functionally graded plates by Carrera's Unified Formulation. Ferreira et al.,[32] Mantari,[33] Amabili et al.[34] also noticed this problem and considered the effect of transverse stretching to analyze the behavior of plates and shells. It is found by comparison that the proposed has relatively simple computational complexity and accurate results can be obtained based on it. In particular, Kiani[35–38] and his collaborators studied the free vibration and dynamic response of graphene platelet reinforced plates using a quasi 3D shear and normal deformable plate model. Through comparison, it was found that the quasi-3D shear deformation theory proposed by Neves et al.[39] can obtain more accurate results. Moreover, the computational complexity of this method is relatively simple.

The effect of several micromechanical models on the free vibration and static behavior of a functionally graded plate is assessed. A quasi-3D hyperbolic shear deformation theory considering the transverse stretching subject to the simply-supported condition is used. These micromechanical models (Voigt, Reuss, Hashin-Shtrikman bounds, LRVE, Tamura) are used to describe the equivalent physical properties of FGMs. The power-law, Sigmoid, and exponential function distributions of volume fraction though thicknesses are considered. The temperature effect of the micromechanical models on the fundamental frequency and transverse displacement for an FGM plate have also been discussed. The influence of different micro mechanical modeling processes on structural deformation and vibration was clearly demonstrated through numerical simulation. This paper provides a theoretical analysis basis for a more accurate mechanical behavior prediction of actual engineering structures.

2. EFFECTIVE MATERIAL PROPERTIES OF FGMS

To solve the mechanical behavior of an FGM structure, it is often assumed that the volume fraction of a component is a continuous variation function along the gradient direction. Based on the equivalent physical parameter model, the variation function of physical parameters is obtained. Many researchers used power-law (P-FGM),[40,41] Sigmoid (S-FGM),[42,43] or exponential (E-FGM)[44,45] and other forms to describe the volume. In this paper, the following three schemes are selected:

$$V(z) = \left(\frac{z}{h} + \frac{1}{2}\right)^n, \quad (P-FGM),$$

$$V(z) = \begin{cases} 1 - \frac{1}{2}\left(\frac{h-2z}{h}\right) & x \le z \le \frac{h}{2} \\ \frac{1}{2}\left(\frac{h+2z}{h}\right)^n & 0 \le z \le \frac{h}{2} > 0 \end{cases}, \quad (S-FGM),$$

$$V(z) = e^{n\left(\frac{z}{h}-1\right)}, \quad (E-FGM); \tag{1}$$

where n is the non-homogeneity index which could be applied to optimize the performance of FGM. The functionally graded plate with uniform thickness h. P-FGM is the simplest model which has been extensively applied in the research. S-FGM is most applicable in layered FGM plates and E-FGM is very common in fracture mechanics. These schemes are necessary to simplify their complicated heterogeneous microstructures to analyze FGMs in an efficient behavior. In this work, five methods (Voigt, Reuss, Hashin-Shtrikman bounds, LRVE, Tamura) are employed to predict the effective material properties of the functionally graded plate.

The Voigt model is the simplest and most common micromechanical to obtain the equivalent macroscopic material properties of the FGM according to the assumption of equal strain, the Young's modulus $E(z)$ and Poisson's ratio $\nu(z)$:

$$\begin{aligned} E(z) &= E_c E(z) + E_m(1 - V(z)), \\ v(z) &= v_c E(z) + v_m(1 - V(z)). \end{aligned} \tag{2}$$

The subscripts "c" and "m" respectively respectively denote the material properties of ceramics and metal. Reuss' mixed law model made the rule of mixture to achieve the effective properties according to the assumption of equal stress as:

$$\begin{aligned} E(z) &= \frac{E_c E_m}{E_c(1 - V(z)) + E_m V(z)}, \\ v(z) &= \frac{v_c v_m}{v_c(1 - V(z)) + v_m V(z)}. \end{aligned} \tag{3}$$

A closed-form expressions for upper and lower bounds of the effective properties using the variational principle by Hashin and Shtrikam. For the lower bound, the effective shear G and bulk K moduli as:

$$\begin{aligned} G_L(z) &= G_m + \frac{V(z)}{\frac{1}{G_c - G_m} + \frac{6(K_m + 2G_m)(1 - V(z))}{5G_m(3K_m + 4G_m)}}, \\ K_L(z) &= K_m + \frac{V(z)}{\frac{1}{K_c - K_m} + \frac{3(1 - V(z))}{(3K_m + 4G_m)}}. \end{aligned} \tag{4}$$

For the upper bound, the effective shear G and bulk K moduli as:[12]

$$\begin{aligned} G_U(z) &= G_c + \frac{1 - V(z)}{\frac{1}{G_m - G_c} + \frac{6(K_c + 2G_c)V(z)}{5G_c(3K_c + 4G_c)}}, \\ K_L(z) &= K_c + \frac{1 - V(z)}{\frac{1}{K_m - K_c} + \frac{3V(z)}{3K_c + 4G_c}}; \end{aligned} \tag{5}$$

$$\begin{aligned} E(z) &= \frac{9G(z)K(z)}{G(z) + 3K(z)}, \\ v(z) &= \frac{3K(z) - 2G(z)}{2(G(z) + 3K(z))}. \end{aligned} \tag{6}$$

Gasik and Lilis used the LRVE method to get the effective material properties of FGM:

$$\begin{aligned} E(z) &= E_m\left(1 + \frac{V(z)}{FE - V(z)^{\frac{1}{3}}}\right), \\ FE &= \frac{1}{1 - E_m/E_c}. \end{aligned} \tag{7}$$

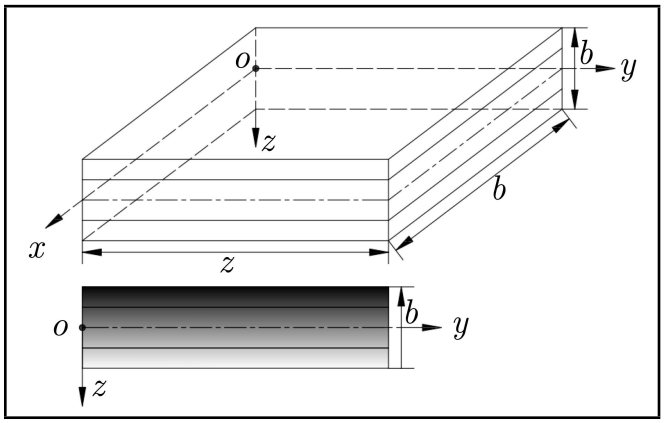

Figure 1. Geometry of functionally graded plate.

The effective Poisson's ratio is the same as Voigt micromechanical scheme. Tamura method made a rule of mixture for effective properties with a fitting parameter q_T known as "stress-to-strain transfer":[13]

$$E(z) = \frac{(1-V(z))E_m\left(q_T - E_c\right) + V(z)E_c\left(q_T - E_m\right)}{(1-V(z))\left(q_T - E_c\right) + V(z)E_c\left(q_T - E_m\right)},$$
$$v(z) = v_c V(z) + v_m(1-V(z)). \tag{8}$$

This method is highly dependent on values of q_T. The $q_T = 0$ could be estimated corresponding to the Reuss rule and $q_T = \infty$ to the Voigt rule. The mass density ρ is obtained:

$$\rho(z) = \rho_c V(z) + \rho_m(1-V(z). \tag{9}$$

3. CONSTITUTIVE RELATION AND BASIC FORMULATION

The plate with coordinate system x, y, z in middle plane ($z = 0$). a, b are the length and width of the plate, respectively in Figure 1. The plate consisting of a mixture of ceramic and metal. A quasi-3D hyperbolic shear deformation theory considering transverse stretching is used:

$$\begin{aligned}
&u(x,y,z,t) = u_0(x,y,t) + zu_1(x,y,t) + \\
&\sinh\left(\frac{\pi z}{h}\right) u_2(x,y,t), \\
&v(x,y,z,t) = v_0(x,y,t) + zv_1(x,y,t) + \\
&\sinh\left(\frac{\pi z}{h}\right) v_2(x,y,t), \\
&w(x,y,z,t) = w_0(x,y,t) + zw_1(x,y,t) + \\
&z^2 w_2(x,y,t);
\end{aligned} \tag{10}$$

where (u, v, w) are the displacement components along (x, y, z) coordinate, (u_0, v_0, w_0) are the displacement components of the middle plane. $u_0, v_0, w_0, u_1, v_1, w_1, u_2, v_2, w_2$ are the functions to be determined depending on x, y, t. The strain-displacement can be written:[39]

$$\begin{Bmatrix} \varepsilon_{xx} \\ \varepsilon_{yy} \\ \gamma_{xy} \end{Bmatrix} = \begin{Bmatrix} \frac{\partial u_0}{\partial x} \\ \frac{\partial v_0}{\partial y} \\ \frac{\partial u_0}{\partial y} + \frac{\partial v_0}{\partial x} \end{Bmatrix} + z \begin{Bmatrix} \frac{\partial u_1}{\partial x} \\ \frac{\partial v_1}{\partial y} \\ \frac{\partial u_1}{\partial y} + \frac{\partial v_1}{\partial x} \end{Bmatrix} + \sinh\left(\frac{\pi z}{h}\right) \begin{Bmatrix} \frac{\partial u_2}{\partial x} \\ \frac{\partial v_2}{\partial y} \\ \frac{\partial u_2}{\partial y} + \frac{\partial v_2}{\partial x} \end{Bmatrix},$$
$$\begin{Bmatrix} \gamma_{xz} \\ \gamma_{yz} \end{Bmatrix} = \begin{Bmatrix} u_1 \\ v_1 \end{Bmatrix} + \cosh\left(\frac{\pi z}{h}\right) \frac{\pi}{h} \begin{Bmatrix} u_z \\ v_z \end{Bmatrix} + \begin{Bmatrix} \frac{\partial w_0}{\partial x} \\ \frac{\partial w_0}{\partial y} \end{Bmatrix} + z \begin{bmatrix} \frac{\partial w_1}{\partial x} \\ \frac{\partial w_1}{\partial y} \end{bmatrix} + z^2 \begin{Bmatrix} \frac{\partial w_2}{\partial x} \\ \frac{\partial w_2}{\partial y} \end{Bmatrix},$$
$$\varepsilon_{zz} = w_1 + 2zw_2; \tag{11}$$

where $\varepsilon_{xx}, \varepsilon_{yy}, \varepsilon_{zz}, \gamma_{xz}, \gamma_{yz}, \gamma_{xy}$ represent strain components. The constitutive relation is:

$$\begin{pmatrix} \sigma_{xx} \\ \sigma_{yy} \\ \sigma_{zz} \\ \tau_{xz} \\ \tau_{yz} \\ \tau_{xy} \end{pmatrix} = \begin{bmatrix} Q_{11} & Q_{12} & Q_{13} & & & \\ Q_{21} & Q_{22} & Q_{23} & & & \\ Q_{31} & Q_{32} & Q_{33} & & & \\ & & & Q_{44} & & \\ & & & & Q_{55} & \\ & & & & & Q_{66} \end{bmatrix} \cdot \left\{ \begin{pmatrix} \varepsilon_{xx} \\ \varepsilon_{yy} \\ \varepsilon_{zz} \\ \gamma_{xz} \\ \gamma_{yz} \\ \gamma_{xy} \end{pmatrix} - \begin{pmatrix} \alpha \\ \alpha \\ \alpha \\ 0 \\ 0 \\ 0 \end{pmatrix} \Delta T \right\}; \tag{12}$$

where $\sigma_{xx}, \sigma_{yy}, \sigma_{zz}, \tau_{xz}, \tau_{yz}, \tau_{xy}$ are the stress components, ΔT is the temperature variation, $Q_{ij}(i,\ j = 1, 2, \ldots, 6)$ are the elastic stiffness components:[39]

$$\begin{aligned}
&Q_{11} = Q_{22} = Q_{33} = \frac{E\left(1-v^2\right)}{1-3v^2-2v^3}, Q_{12} = Q_{21} = \\
&\frac{E\left(v+v^2\right)}{1-3v^2-2v^3}, \\
&Q_{13} = Q_{31} = \frac{E\left(v+v^2\right)}{1-3v^2-2v^3}, Q_{23} = Q_{32} = \\
&\frac{E\left(v+v^2\right)}{1-3v^2-2v^3}, \\
&Q_{44} = Q_{55} = Q_{66} = \frac{E}{2(1+v)}.
\end{aligned} \tag{13}$$

By the principle of virtual displacement, we can obtain the following equations:

$$\begin{aligned}
&N_{xy,y} + N_{xx,x} = I_0\ddot{u}_0 + I_1\ddot{u}_1 + I_7\ddot{u}_2, \\
&N_{yy,y} + N_{xy,x} = I_0\ddot{v}_0 + I_1\ddot{v}_1 + I_7\ddot{v}_2, \\
&N_{xz,x} + N_{yz,y} - q = I_0\ddot{w}_0 + I_1\ddot{w}_1 + I_2\ddot{w}_2, \\
&N_{xz} - M_{xy,y} - M_{xx,x} = -I_1\ddot{u}_0 - I_2\ddot{u}_1 - I_5\ddot{u}_2, \\
&N_{yz} - M_{xy,x} - M_{yy,y} = -I_1\ddot{v}_0 - I_2\ddot{v}_1 - I_5\ddot{v}_2, \\
&N_{zz} - M_{xz,x} - M_{yz,y} - qz = -I_1\ddot{w}_0 - I_2\ddot{w}_1 - I_3\ddot{w}_2, \\
&S_{xz} - P_{xy,y} - P_{xx,x} = -I_7\ddot{u}_0 - I_5\ddot{u}_1 - I_6\ddot{u}_2, \\
&S_{yz} - P_{xy,x} - P_{yy,y} = -I_7\ddot{v}_0 - I_5\ddot{v}_1 - I_6\ddot{v}_2, \\
&2M_{zz} - O_{xz,x} - O_{yz,y} - qz^2 = -I_2\ddot{w}_0 - I_3\ddot{w}_1 - I_4\ddot{w}_2.
\end{aligned} \tag{14}$$

The following stress resultants are considered:

$$
\begin{aligned}
&\{N_{xx}N_{yy}N_{zz}N_{xz}N_{yz}N_{xy}\} = \\
&\int_{-h/2}^{h/2} \{\sigma_{xx}\sigma_{yy}\sigma_{zz}\tau_{xz}\tau_{yz}\tau_{xy}\}\, dz, \\
&\{M_{xx}M_{yy}M_{zz}M_{xz}M_{yz}M_{xy}\} = \\
&\int_{-h/2}^{h/2} z\,\{\sigma_{xx}\sigma_{yy}\sigma_{zz}\tau_{xz}\tau_{yz}\tau_{xy}\}\, dz, \\
&\{O_{xx}O_{yy}O_{zz}O_{xz}O_{yz}O_{xy}\} = \\
&\int_{-h/2}^{h/2} z^2\,\{\sigma_{xx}\sigma_{yy}\sigma_{zz}\tau_{xz}\tau_{yz}\tau_{xy}\}\, dz, \\
&\{P_{xx}P_{yy}P_{zz}P_{xz}P_{yz}P_{xy}\} = \\
&\int_{-h/2}^{h/2} \sinh\left(\frac{\pi z}{h}\right)\{\sigma_{xx}\sigma_{yy}\sigma_{zz}\tau_{xz}\tau_{yz}\tau_{xy}\}\, dz, \\
&\{S_{xx}S_{yy}S_{zz}S_{xz}S_{yz}S_{xy}\} = \\
&\int_{-h/2}^{h/2} \frac{\pi}{h}\sinh\left(\frac{\pi z}{h}\right)\{\sigma_{xx}\sigma_{yy}\sigma_{zz}\tau_{xz}\tau_{yz}\tau_{xy}\}\, dz, \\
&\{I_0, I_1, I_2, I_3, I_4\} = \int_{-h/2}^{h/2} \rho_0\left\{1 z z^2 z^3 z^4\right\} dz, \\
&\{I_5, I_6, I_7\} = \\
&\int_{-h/2}^{h/2} \rho_0\left\{\sinh\left(\frac{\pi z}{h}\right)\cdot z\sinh\left(\frac{\pi z}{h}\right)^2 \sinh\left(\frac{\pi z}{h}\right)\right\} dz.
\end{aligned}
\tag{15}
$$

$q = \sum_{i=1}^{\infty}\sum_{j=1}^{\infty} q_0 \sin(\alpha x)\sin(\beta y)$ is the distributed transverse load.

4. NUMERICAL METHODOLOGY OF SOLUTION

Considering the FGM plate under the simply supported boundary conditions:

$$
\begin{aligned}
&x = 0, a : N_{xx} = M_{xx} = v_0 = w_0 = v_1 = v_2 = w_2 = 0, \\
&y = 0, b : N_{yy} = M_{yy} = u_0 = w_0 = u_1 = u_2 = w_1 = 0.
\end{aligned}
\tag{16}
$$

Based on the above conditions, by using Navier method, the approximate solutions can be represented as the following Fourier series:

$$
\begin{Bmatrix} u_0 \\ v_0 \\ w_0 \\ u_1 \\ v_1 \\ w_1 \\ u_2 \\ v_2 \\ w_2 \end{Bmatrix} = \sum_{m=1}^{\infty}\sum_{n=1}^{\infty} \begin{Bmatrix} U_{mn}^0 \cos(\alpha x)\sin(\beta y) \\ V_{mn}^0 \sin(\alpha x)\cos(\beta y) \\ W_{mn}^0 \sin(\alpha x)\sin(\beta y) \\ U_{mn}^1 \cos(\alpha x)\sin(\beta y) \\ V_{mn}^1 \sin(\alpha x)\cos(\beta y) \\ W_{mn}^1 \sin(\alpha x)\sin(\beta y) \\ U_{mn}^2 \cos(\alpha x)\sin(\beta y) \\ V_{mn}^2 \sin(\alpha x)\cos(\beta y) \\ W_{mn}^2 \sin(\alpha x)\sin(\beta y) \end{Bmatrix} e^{i\omega t}; \tag{17}
$$

where $i = \sqrt{-1}, \alpha = \frac{m\pi}{a}, \beta = \frac{n\pi}{b}$, $\Delta^T = \left\{U_{mn}^0, V_{mn}^0, W_{mn}^0, U_{mn}^1, V_{mn}^1, W_{mn}^1, W_{mn}^2, U_{mn}^2, V_{mn}^2,\right\}$ are the coefficients to be determined.

5. RESULTS AND DISCUSSIONS

5.1. Effect of Micromechanical Schemes

The response of FGM plates with a metal (Al) top surface and ceramic (Al_20_3) bottom surface are estimated by five micromechanical models. The impacts of five effective micromechanical schemes have been examined. The non-homogeneity index n, the aspect ratio b/a on the static deflection (displacements, stresses, maximum deflection) are discussed. The material parameters are used of $E_c = 380$ GPa, $E_m = 69$ GPa, $\rho_c = 3980$ kg/m^3, $\rho_m = 2710$ kg/m^3, $\nu_c = 0.22$, $\nu_m = 0.33$. The dimensionless natural frequency Ω, the non-dimensional transverse deflection W, the non-dimensional displacements u, v, w and stresses τ_{xy}, τ_{yz} of system are calculated as following non-dimensional form:

$$
\begin{aligned}
&\Omega = \frac{\omega a^2}{h}\sqrt{\frac{\rho_m}{E_m}}, \quad W = w_0\frac{E_m h^3}{a^4 q_0}, \\
&v = v\left(\frac{a}{2}, 0, z\right)\frac{10E_b h^3}{q_0 a^4}, \\
&w = w\left(\frac{a}{2}, \frac{b}{2}, z\right)\frac{10E_b h^3}{q_0 a^4}, \\
&\tau_{xy} = \tau_{xy}(0,0,z)\frac{10h^2}{q_0 a^2}, \quad \tau_{yz} = \tau_{yz}\left(\frac{a}{2}, 0, z\right)\frac{h}{q_0 a}.
\end{aligned}
\tag{18}
$$

The free vibration of FGM plates is obtained by using the quasi-3D hyperbolic shear deformation theory. The present results of five models are verified by TSDT and CLPT comparing with literature.[17] Table 1 shows the non-dimensional fundamental frequency of the P-FGM volume fraction scheme considering the thickness-to-side ratios $a/h = 5, 10, 100$, the non-homogeneity indices $n = 0, 0.5, 1, 2, 10, \infty$ and the fitting parameter $q_T = -100$ GPa. Under different micro mechanical models, the fundamental frequency of the theory we used is consistent with the known theory. Furthermore, the numerical results were relatively small, as the theory used considers the stretching effect, which makes the results more accurate. The dimensionless fundamental frequency increases monotonically with the thickness-to-side ratio and decreases with the non-homogeneity index. The maximum and minimum value of free vibration response appear in the Voigt and Reuss method respectively. The changes of the fundamental frequencies are almost consistent with the non-homogeneity index in Tamura, LRVE, Hashin (LB) micromechanical methods. The frequency as Hashin (UB) model is only slightly lower than the value as Voigt model and higher than other models.

The influence of the non-homogeneity index n, the aspect ratio b/a, the thickness-to-side ratios a/h on the fundamental frequencies are investigated in Figures 2–4. By raising the non-homogeneity index and the aspect ratio, these models are dramatically reduced which coincides with the results predicted. For a moderately thick $(a/h = 10)$ homogeneous plate, the fundamental frequency up to 36.1%, 41.97%, 39.67%, 39.68%, 40.06%, 37.76% are respectively from $n = 0$ to $n = 10$. The frequency up to 47.88%, 47.72%, 47.77%, 47.76%, 47.76%, 47.83% are respectively from $b/a = 1$ to $b/a = 6$. The change of frequency under different schemes is consistent with the increase of the aspect ratio. The aspect ratio has little influence on the frequency of

Table 1. Non-dimensional fundamental frequency Ω estimated by several micromechanical models.

a/h	n	Voigt			Reuss			Tamura		
		present	TSDT[17]	CLPT[17]	present	TSDT[17]	CLPT[17]	present	TSDT[17]	CLPT[17]
5	0	9.9001	10.0885	10.9571	9.9001	10.0885	10.9571	9.9001	10.0885	10.9571
	0.5	8.4937	8.7277	9.4189	6.9393	7.1185	7.7166	7.5178	7.7238	8.3444
	1	7.6822	7.9227	8.5358	6.4507	6.6432	7.2682	6.8742	7.0879	7.6978
	2	6.9517	7.1877	7.7910	6.1365	6.3369	7.0298	6.4290	6.6446	7.3149
	10	6.1604	6.3804	7.2220	5.6444	5.8474	6.5423	5.8448	6.0556	6.8144
	∞	5.0846	5.3172	5.8472	5.0846	5.3172	5.8472	5.0846	5.3172	5.8472
10	0	10.7055	10.9548	11.2199	10.7055	10.9548	11.2199	10.7055	10.9548	11.2199
	0.5	9.1333	9.4370	9.6468	7.4961	7.7349	7.9193	8.0963	8.3671	8.5569
	1	8.2531	8.5671	8.7542	7.0076	7.2673	7.4621	7.4291	7.7141	7.9028
	2	7.5049	7.8215	8.0089	6.7236	6.9987	7.2176	7.0111	7.3059	7.5170
	10	6.8405	7.1517	7.4243	6.2121	6.4889	6.7091	6.4585	6.7503	6.9927
	∞	5.5191	5.8237	5.9875	5.5191	5.8237	5.9875	5.5191	5.8237	5.9875
100	0	11.0320	11.3080	11.3109	11.0320	11.3080	11.3109	11.0320	11.3080	11.3109
	0.5	9.3888	9.7234	9.7256	7.7210	7.9873	7.9893	8.3283	8.6283	8.6303
	1	8.4807	8.8277	8.8297	7.2360	7.5270	7.5291	7.6534	7.9716	7.9737
	2	7.7284	8.0824	8.0844	6.9691	7.2802	7.2826	7.2521	7.5847	7.5870
	10	7.1343	7.4913	7.4943	6.4517	6.7644	6.7669	6.7200	7.0519	7.0545
	∞	5.6966	6.0342	6.0360	5.6966	6.0342	6.0360	5.6966	6.0342	6.0360
a/h	n	LRVE			Hashin (LB)			Hashin (UB)		
		present	TSDT[17]	CLPT[17]	present	TSDT[17]	CLPT[17]	present	TSDT[17]	CLPT[17]
5	0	9.9001	10.0885	10.9571	9.9001	10.0885	10.9571	9.9001	10.0885	10.9571
	0.5	7.5114	7.7172	8.3253	7.4153	7.6305	8.2564	8.0294	8.2334	8.8759
	1	6.8434	7.0561	7.6542	6.7963	7.0157	7.6362	7.2811	7.4944	8.0892
	2	6.4125	6.6273	7.3025	6.3760	6.5952	7.2771	6.6965	6.9152	7.5417
	10	5.8420	6.0524	6.8137	5.8110	6.0267	6.7778	6.0130	6.2222	7.0248
	∞	5.0846	5.3172	5.8472	5.0846	5.3172	5.8472	5.0846	5.3172	5.8472
10	0	10.7055	10.9548	11.2199	10.7055	10.9548	11.2199	10.7055	10.9548	11.2199
	0.5	8.0821	8.3524	8.5382	7.9922	8.2757	8.4676	8.6342	8.9005	9.0959
	1	7.3911	7.6751	7.8601	7.3542	7.6475	7.8399	7.8374	8.1188	8.3012
	2	6.9983	7.2932	7.5063	6.9624	7.2623	7.4775	7.2604	7.5569	7.7527
	10	6.4576	6.7486	6.9920	6.4171	6.7147	6.9544	6.6630	6.9562	7.2143
	∞	5.5191	5.8237	5.9875	5.5191	5.8237	5.9875	5.5191	5.8237	5.9875
100	0	11.0320	11.3080	11.3109	11.0320	11.3080	11.3109	11.0320	11.3080	11.3109
	0.5	8.3104	8.6098	8.6118	8.2240	8.5385	8.5406	8.8760	9.1698	9.1719
	1	7.6128	7.9293	7.9313	7.5807	7.9082	7.9103	8.0605	8.3726	8.3745
	2	7.2414	7.5745	7.5768	7.2060	7.5444	7.5468	7.4910	7.8237	7.8258
	10	6.7201	7.0510	7.0537	6.6749	7.0130	7.0156	6.9419	7.2771	7.2790
	∞	5.6966	6.0342	6.0360	5.6966	6.0342	6.0360	5.6966	6.0342	6.0360

different schemes. The predicted results of these models increase by raising the thickness-to-side ratios. The frequency up to 11.07%, 13.44%, 12.68%, 12.81%, 12.89%, 11.75% are respectively from $a/h = 5$ to $a/h = 50$. The thickness-to-side ratio plays a major role on the free vibration. The maximum and minimum non-dimensionalized fundamental frequencies are in the Voigt and Reuss method respectively. All values tend to be stable with the increase of three types of parameters in micromechanical models.

The maximum deflection under uniform static load estimated by several micromechanical models in Table 2. The maximum non-dimensional deflection increases monotonically with the non-homogeneity index and decreases with the thickness-to-side ratio. The maximum non-dimensional deflection with the theory we employed are consistent with the known theory. The numerical results are smaller because of the thickness stretching effect serves to make the plate stiffness, which leads to a reduction of deflection.

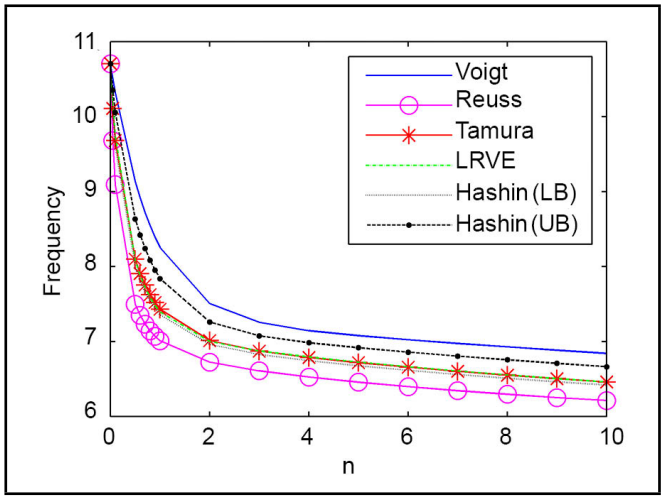

Figure 2. Non-dimensionalized fundamental frequencies of the non-homogeneity index.

The non-dimensional deflection under uniform static load with the non-homogeneity index $n = 2$ and the thickness-to-side ratio $a/h = 4$ are shown in Figures 5 and 6. Figures 7 and 8 estimate the distribution of the shear stresses $\tau_{xy}(0, 0, z)$, $\tau_{yz}(a/2, 0, z)$ through the thickness of FGM plates. The Voigt and Reuss models provide the lower and upper bounds of the

Table 2. Maximum non-dimensional deflection ($W \times 1000$) under uniform static load estimated by several micromechanical models.

a/h	n	Voigt			Reuss			Tamura		
		present	TSDT[17]	CLPT[17]	present	TSDT[17]	CLPT[17]	present	TSDT[17]	CLPT[17]
5	0	6.5694	9.9796	8.6209	6.5694	9.9796	8.6209	6.5694	9.9796	8.6209
	0.5	9.9474	14.9113	13.0495	14.8573	22.3403	19.3436	12.6662	18.9980	16.5749
	1	12.8740	19.1894	16.8376	18.2745	27.2708	23.1595	16.0673	23.9452	20.6500
	2	16.7137	24.7938	21.4493	21.6004	32.0171	26.4230	19.6145	29.063	24.3500
	10	23.8191	34.9869	27.6679	28.4607	41.7976	33.9279	26.5283	38.9400	31.2192
	∞	36.5073	52.7839	44.4589	36.5073	52.7839	44.4589	36.5073	52.7839	44.4589
10	0	5.8416	8.8105	8.6209	5.8416	8.8105	8.6209	5.8416	8.8105	8.6209
	0.5	8.9730	13.2870	13.0495	13.3041	19.7509	19.3436	11.4092	16.8889	16.5749
	1	11.6695	17.1282	16.8376	16.1793	23.7772	23.1595	14.3936	21.1072	20.6500
	2	15.0415	21.9014	21.4493	18.7642	27.3563	26.4230	17.2438	25.096	24.3500
	10	20.1024	29.0130	27.6679	24.4111	35.3068	33.9279	22.5753	32.6065	31.2192
	∞	32.2543	45.7670	44.4589	32.2543	45.7670	44.4589	32.2543	45.7670	44.4589
100	0	5.5948	8.4241	8.6209	5.5948	8.4241	8.6209	5.5948	8.4241	8.6209
	0.5	8.6427	12.7502	13.0495	12.7782	18.8949	19.3436	10.9835	16.1918	16.5749
	1	11.2619	16.4470	16.8376	15.4699	22.6221	23.1595	13.8272	20.1690	20.6500
	2	14.4764	20.9452	21.4493	17.8031	25.8149	26.4230	16.4410	23.7842	24.3500
	10	18.8410	27.0369	27.6679	23.0389	33.16	33.9279	21.2352	30.5116	31.2192
	∞	30.8126	43.4475	44.4589	30.8126	43.4475	44.4589	30.8126	43.4475	44.4589
a/h	n	LRVE			Hashin (LB)			Hashin (UB)		
		present	TSDT[17]	CLPT[17]	present	TSDT[17]	CLPT[17]	present	TSDT[17]	CLPT[17]
5	0	6.5694	9.9796	8.6209	6.5694	9.9796	8.6209	6.5694	9.9796	8.6209
	0.5	12.6817	19.0247	16.6468	13.0148	19.4628	16.9256	11.1202	16.7373	14.6739
	1	16.1995	24.1483	20.8721	16.4396	24.4424	20.9825	14.3239	21.4247	18.7196
	2	19.7083	29.2035	24.4164	19.9529	29.5094	24.6096	18.0371	26.7988	22.8888
	10	26.5576	38.9849	31.2264	26.8392	39.3203	31.5664	25.0391	36.8419	29.3179
	∞	36.5073	52.7839	44.4589	36.5073	52.7839	44.4589	36.5073	52.7839	44.4589
10	0	5.8416	8.8105	8.6209	5.8416	8.8105	8.6209	5.8416	8.8105	8.6209
	0.5	11.4481	16.9479	16.6468	11.7065	17.2617	16.9256	10.0373	14.9324	14.6739
	1	14.5387	21.3197	20.8721	14.6875	21.4750	20.9825	12.9366	19.0641	18.7196
	2	17.3041	25.1790	24.4164	17.4877	25.3981	24.6096	16.0740	23.4578	22.8888
	10	22.5822	32.6231	31.2263	22.8687	32.9562	31.5664	21.2009	30.6876	29.3179
	∞	32.2543	45.7670	44.4589	32.2543	45.7670	44.4589	32.2543	45.7670	44.4589
100	0	5.5948	8.4241	8.6209	5.5948	8.4241	8.6209	5.5948	8.4241	8.6209
	0.5	11.0304	16.2616	16.6468	11.2635	16.5342	16.9256	9.6704	14.3359	14.6739
	1	13.9768	20.3847	20.8721	14.0945	20.4940	20.9825	12.4673	18.2838	18.7196
	2	16.4899	23.8481	24.4164	16.6528	24.0385	24.6096	15.4100	22.3531	22.8888
	10	21.2345	30.5188	31.2263	21.5229	30.8511	31.5664	19.8988	28.6518	29.3179
	∞	30.8126	43.4475	44.4589	30.8126	43.4475	44.4589	30.8126	43.4475	44.4589

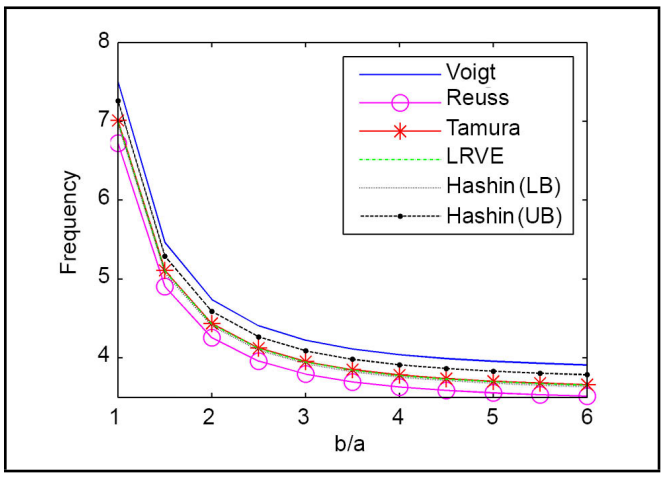

Figure 3. Non-dimensionalized fundamental frequencies of the aspect ratio.

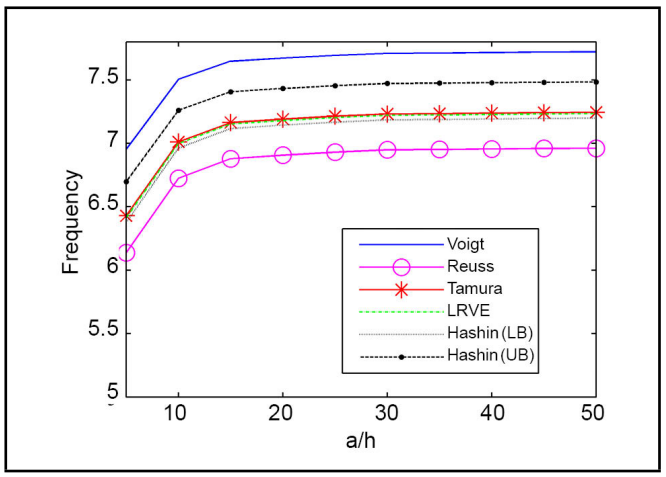

Figure 4. Non-dimensionalized fundamental frequencies the thickness-to-side ratios.

displacements and stresses. The deflection results of transverse displacement are much larger than that in plane displacement. The numerical disparity of transverse displacement under different schemes is also great. The influence of the non-homogeneity index n, the aspect ratio b/a on the maximum non-dimensional deflection are investigated in Figures 9 and 10 with the thick plate $a/h = 4$ and $a/h = 10$, respectively. The maximum non-dimensional deflections are 31.71%,

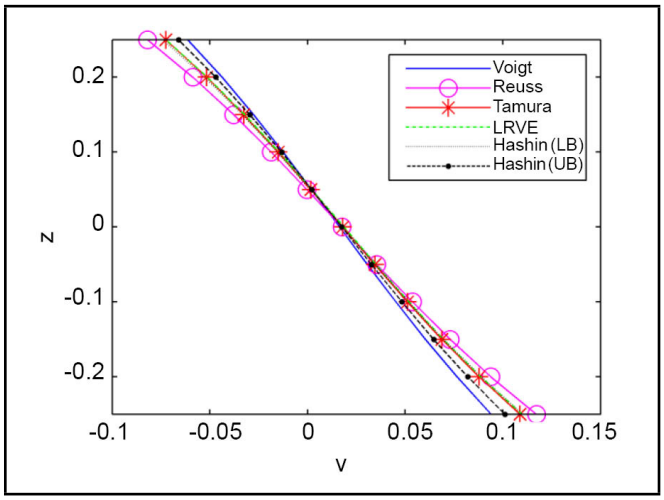

Figure 5. Distribution of non-dimensionalized displacement v through the thickness.

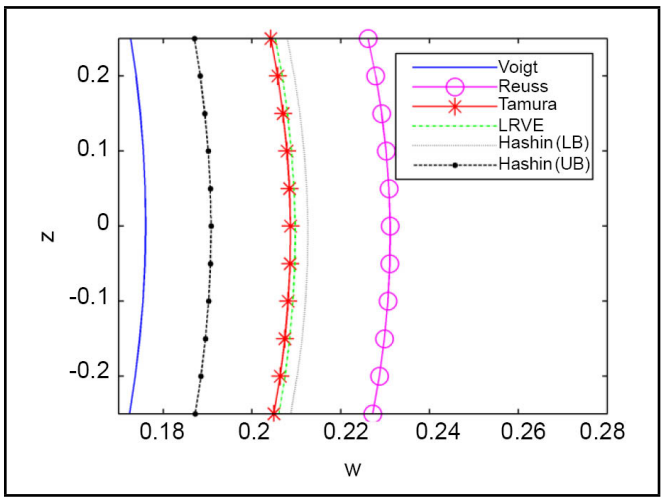

Figure 6. Distribution of non-dimensionalized displacement w through the thickness.

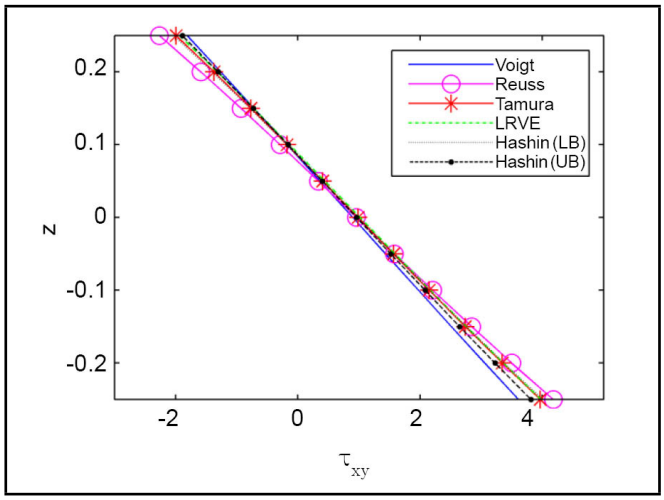

Figure 7. Distribution of non-dimensionalized shear stress τ_{xy} through the thickness.

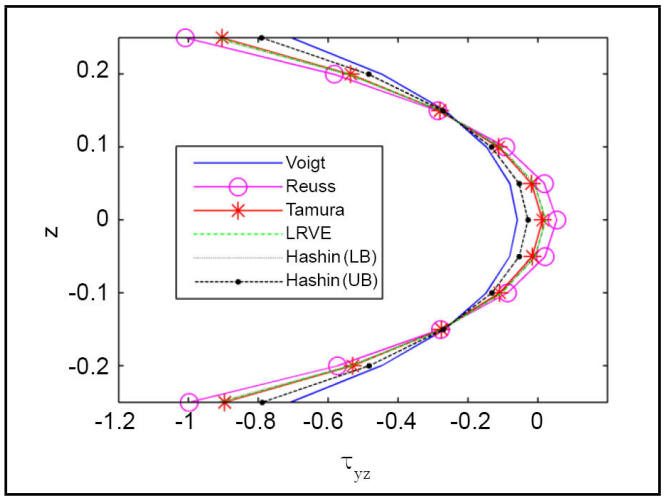

Figure 8. Distribution of non-dimensionalized shear stress τ_{yz} through the thickness.

18.86%, 19.47%, 21.10%, 8.47% higher than the Voigt with $n = 2$. They are: 23.94%, 14.15%, 14.52%, 15.70%, 6.69%, and are higher than the Voigt with $b/a = 4$ using the other micromechanical schemes, respectively.

The Hashin (LB) and Hashin (UB) scheme are often used in accurate bounds of response domain of FGM structures. It is shown that in Table 1, for the moderately thick plate with the thickness-to-side ratio is $a/h = 10$ and the non-homogeneity index $n = 0.5$, the Hashin (LB) and the Hashin (UB) predict the fundamental frequencies to be 12.49%, 5.46% lower than the Voigt model, respectively. On the contrary, the maximum non-dimensional deflection by the Hashin (LB) and Hashin (UB) is 30.46%, 11.86% higher than the Voigt estimation in the same condition. Therefore, it is necessary to choose the appropriate micromechanical modeling of FGM structures to estimate the response.

5.2. Effect of FGM Profiles

The volume fraction distribution alters the material composition of FGM structures and affects the structural behavior. The profile of FGM plates determines the distribution function of volume fraction as Eq. (1). The non-homogeneity index of the volume fraction distribution alters the material composition of FGMs and affects the structural behavior of FGM structures. As shown in Figure 11, to examine the effect of FGM profiles on the free vibration performance of FGM plates, the fundamental frequency with $a/h = 10$ is compared to the P-FGM, S-FGM and E-FGM profiles. The variation of volume fraction by the non-homogeneity index n in an E-FGM profile is more obvious than the S-FGM compared to the P-FGM. The variation of volume fraction by the non-homogeneity index n in S-FGM profile is not remarkable. This is because the exponential functions used in E-FGM plates to describe the variation of Young's modulus throughout the thickness direction. When $n < 1$, the minimum frequency in S-FGM profile, however, it is greater than others as $n > 1$. The discrepancies of non-dimensionalized fundamental frequency up to 36.1%, 48.30%, 19.72% from $n = 0$ to $n = 10$ are respectively estimated by the P-FGM, E-FGM, S-FGM profiles. The influence of the aspect ratio b/a, the thickness-to-side ratios a/h on the non-dimensionalized fundamental frequencies are investigated in Figures 12–13 by the above three types of profiles. For a moderately thick $(a/h = 10)$ homogeneous plate in Figure 12, the discrepancies of frequency up to 47.88%, 47.81%, 47.99% from $b/a = 1$ to $b/a = 6$ are respectively estimated by the P-FGM, E-FGM, S-FGM profiles. The results predicted by those

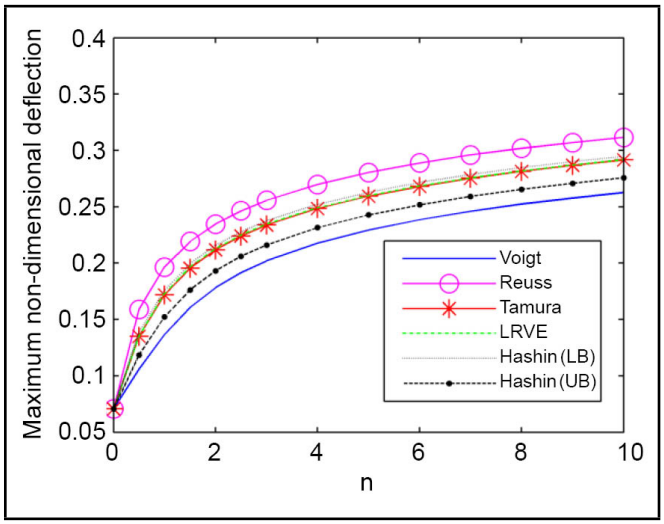

Figure 9. Maximum non-dimensional deflection of non-homogeneity index.

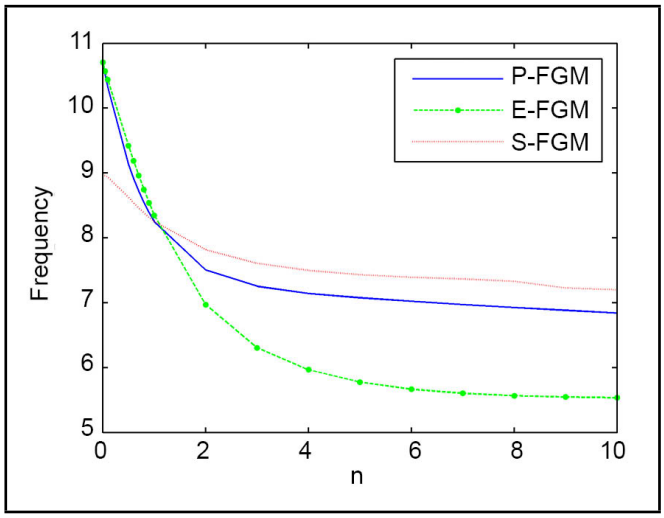

Figure 11. Non-dimensionalized fundamental frequencies of the non-homogeneity index.

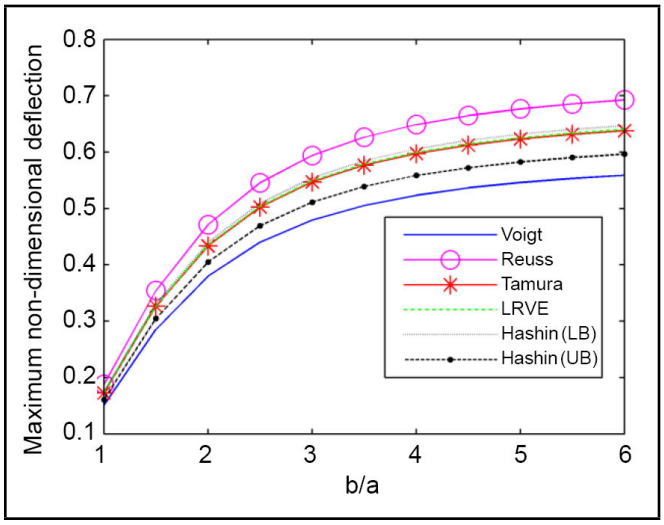

Figure 10. Maximum non-dimensional deflection of the aspect ratio.

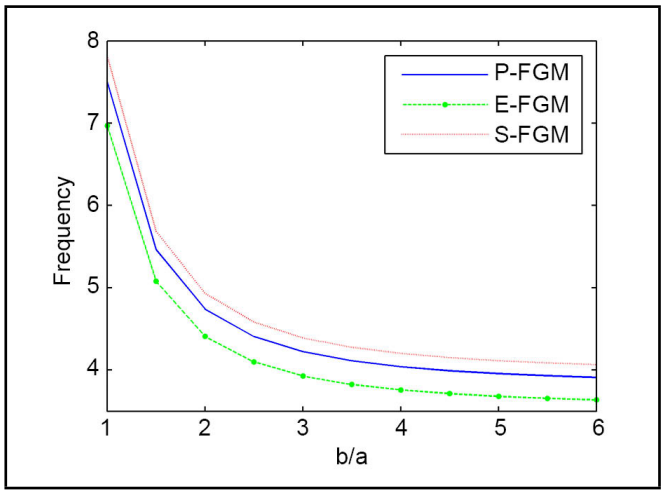

Figure 12. Non-dimensionalized fundamental frequencies of the aspect ratio.

profiles augment by raising the thickness-to-side ratios in Figure 13. The discrepancies of frequency up to 11.07%, 12.11%, 9.34% from $a/h = 5$ to $a/h = 50$ are respectively estimated by the above profiles.

The dimensionless deflections and dimensionless stresses of the FGM plate using power-law, sigmoid and exponential functions are compared in Figures 14–16. The three idealization techniques are thus compared for a uniform static load. The distributions of the plane displacement and transverse displacement through the thickness are seen in Figures 14 and 15. We can see the maximum deflection through the thickness in the E-FGM and the minimum in S-FGM profiles for $a/h = 4$ and $n = 2$, respectively. Figure 15 shows the distribution of shear stress $\tau_{yz}(0, b/2, z)$ through the thickness of FGM plates and were predicted by the Voigt model. We can see the maximum deflection through the thickness in the E-FGM obviously. As seen in Figures 17–18, increasing the non-homogeneity index n and the aspect ratio b/a on the maximum non-dimensional deflection under uniform static load are investigated by three FGM profiles. Figure 17 assuming the thickness-to-side ratio is $a/h = 4$. Figure 18 assuming the thickness-to-side ratio is $a/h = 10$. The discrepancies between the estimated the maximum non-dimensional deflection of FGM plates by the E-FGM and S-FGM profiles with the non-homogeneity index $n = 2$ are higher by 29.01% and lower by 16.44% than the P-FGM profile, respectively in Figure 17. The discrepancies between the estimated the maximum non-dimensional deflection of FGM plate by the E-FGM and S-FGM profiles with the non-homogeneity index $b/a = 4$ are higher by 24.57% and lower by 13.30% than the P-FGM profile, respectively in Figure 18. Therefore, the FGM profiles are important to stimulate the application of the FGM structure performance.

5.3. Effect of Temperature

FGM structures are mainly designed for high temperature environments. The influence of temperature plays a crucial role in evaluating the performance. Assuming the FGM profile is P-FGM, the effect of the temperature of a functionally graded plate is reported. The Voigt, Reuss, Tamura micromechanical models are used to predict the material properties P (including the Young's modulus E and Poisson's ratio ν). The top surface is ceramic (Si_3N_4) and the bottom surface is metal $(SUS304)$. P_c and P_m are denoted as the material properties of ceramic and metal. The thermal expansion coefficients are

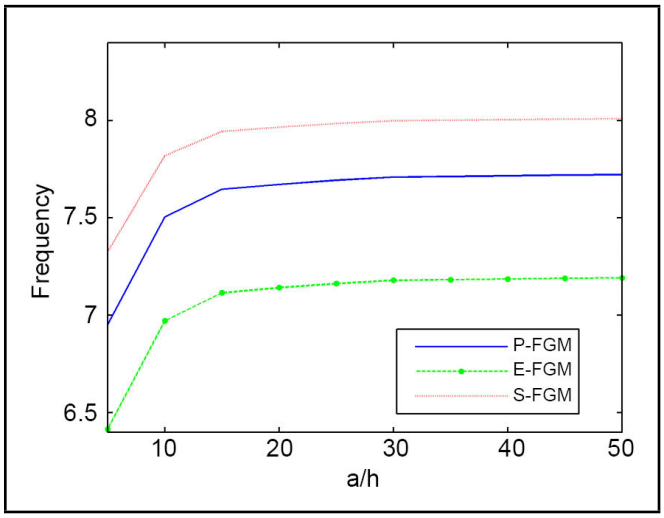

Figure 13. Non-dimensionalized fundamental frequencies the thickness-to-side ratios.

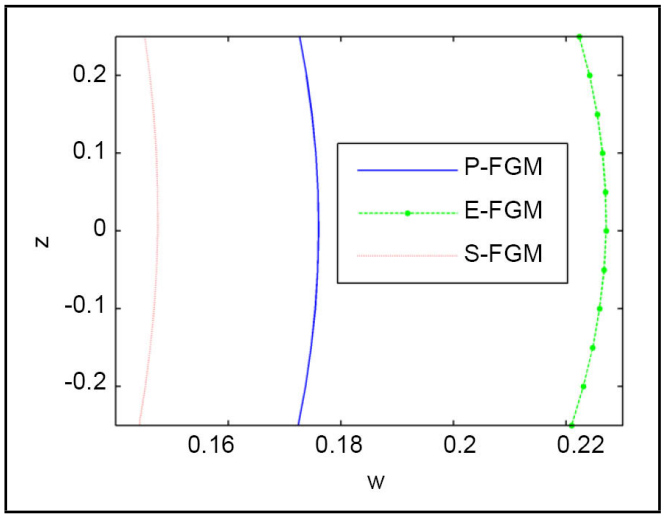

Figure 15. Distribution of non-dimensionalized displacement w through the thickness.

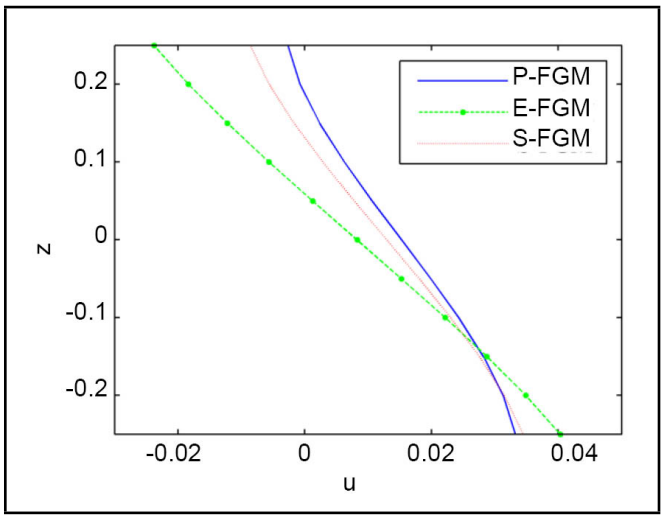

Figure 14. Distribution of non-dimensionalized displacement u through the thickness.

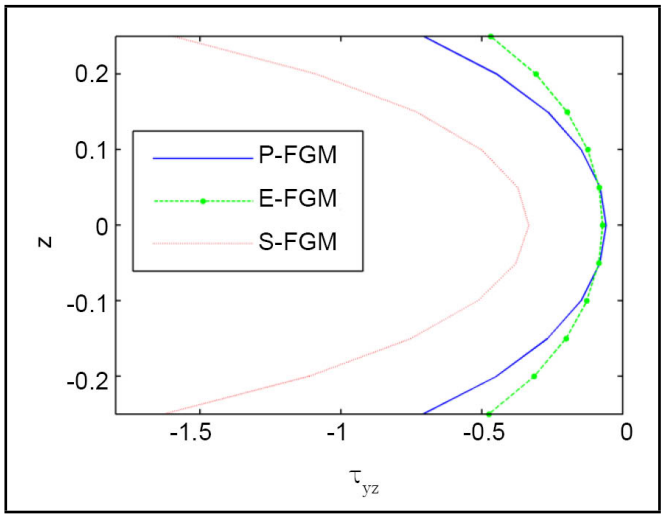

Figure 16. Distribution of non-dimensionalized shear stress τ_{yz} through the thickness.

expressed as:

$$P_i = P_0\left(P_{-1}T^{-1} + 1 + P_1T + P_2T^2 + P_3T^3\right),\ i = c, m; \tag{19}$$

where $P_{-1}, P_0, P_1, P_2, P_3$ are the constant coefficients in the cubic expression of the respective temperature-dependent material property. Where $T = T_l + (T_u - T_l)\,\eta(z)$ denotes the temperature at any point along the thickness direction of the plate in environmental temperature, T_l is the bottom surface temperature of the plate, T_u is the top surface temperature of the plate.

$$\eta(z) = \frac{1}{C}\left[\left(\frac{Z}{h}+\frac{1}{2}\right) - \frac{k_{cm}}{k_m(n+1)}\left(\frac{Z}{h}+\frac{1}{2}\right)^{(n+1)} + \frac{k_{cm}^2}{k_m^2(2n+1)}\left(\frac{Z}{h}+\frac{1}{2}\right)^{(2n+1)} - \frac{k_{cm}^3}{k_m^3(3n+1)}\left(\frac{Z}{h}+\frac{1}{2}\right)^{(3n+1)} + \frac{k_{cm}^4}{k_m^4(4n+1)}\cdot\left(\frac{Z}{h}+\frac{1}{2}\right)^{(4n+1)} - \frac{k_{cm}^5}{k_m^5(5n+1)}\left(\frac{Z}{h}+\frac{1}{2}\right)^{(5n+1)}\right]; \tag{20}$$

$$k_{cm} = k_c - k_m; \tag{21}$$

$$C = 1 - \frac{k_{cm}}{(n+1)k_m} + \frac{k_{cm}^2}{(2n+1)k_m^2} - \frac{k_{cm}^3}{(3n+1)k_m^3} + \frac{k_{cm}^4}{(4n+1)k_m^4} - \frac{k_{cm}^5}{(5n+1)k_m^5}. \tag{22}$$

K_m represents the thermal conductivity of metal materials. K_c represents the thermal conductivity of ceramic materials. Table 3 is the temperature-dependent material coefficients for Si_3N_4 and $SUS304$.

The temperature of the lower surface ($z = -h/2$) is constant at $T_l = 300$ K. Three different temperatures of 300 K, 400 K and 600 K are considered for the upper surface ($z = h/2$). Table 4 exhibits the comparison of non-dimensional frequency parameter $\Omega = \omega\left(a^2/h\right)\sqrt{\rho_m\left(1-v_m^2\right)/E_m}$ for different temperatures with volume faction index n. The non-dimensional frequency equation has a minor difference, other non-dimensional equations have no change. The geometric properties of the plate are as follows: $h = 0.025$ m, $a = b = 0.2$ m. We can see from Table 4 that those three micromechanical moles are in good agreement with literature[46] for different

Table 3. Temperature-dependent material coefficients for Si_3N_4 and SUS304

Material	Symbol	P_0	P_{-1}	P_1	P_2	P_3
Si_3SN_4	$E_c(Pa)$	348.43×10^9	0	-3.070×10^{-4}	2.160×10^{-7}	-8.946×10^{-11}
	$\alpha_c(1/K)$	5.8726×10^{-6}	0	9.095×10^{-4}	0	0
	rho_c (kg/m^3)	2370	0	0	0	0
	K_c (W/mk)	9.19	0	0	0	0
$SUS304$	E_m (Pa)	201.04×10^9	0	3.079×10^{-4}	-6.534×10^{-7}	0
	α_m (1/K)	12.33×10^{-6}	0	8.086×10^{-4}	0	0
	ρ_m (kg/m^3)	8166	0	0	0	0
	K_m (W/mk)	12.04	0	0	0	0

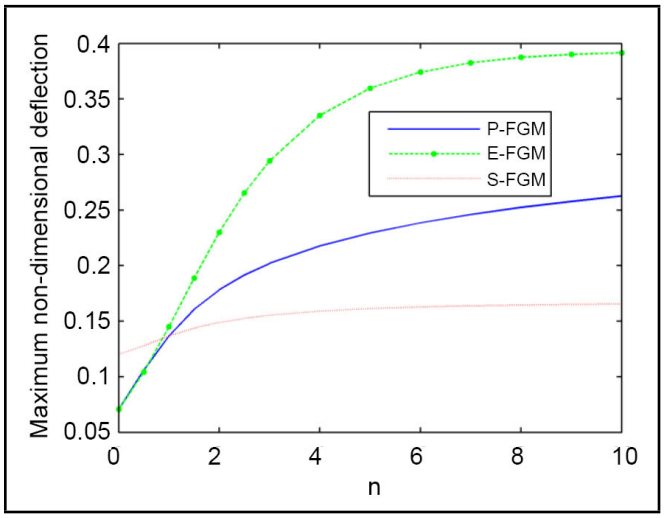

Figure 17. Maximum non-dimensional deflection of non-homogeneity index.

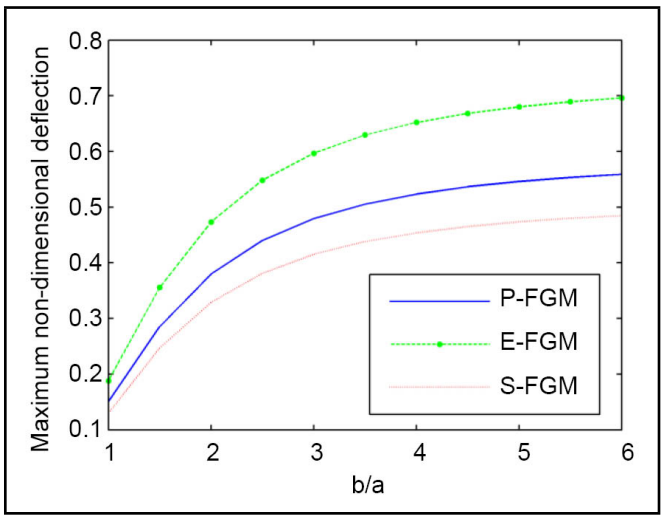

Figure 18. Maximum non-dimensional deflection of the aspect ratio.

values of n and thermal conditions.

Figures 19–20 illustrate the effect of temperature ($\Delta T = T_u - T_l$) on the free vibration of the FGM plate with a different non-homogeneity index $n = 0.5$, 2, 5 and a different aspect ratio $b/a = 1, 2, 4$. The material stiffness of the functionally graded plate decreases and the frequency of the system decreases with increased temperature. The influence of the non-homogeneity index n with various temperature parameter ΔT is shown in Figure 19. An increment occurs for the results as n decreases. When the temperature parameter $\Delta T = 300$ K, the frequency lowers to 1.28%, 0.93% than the Voigt by the other models predicted with the non-homogeneity index $n = 0.5$, lowers to 0.84%, 0.60% with $n = 2$ and lowers to 0.84%, 0.60% with $n = 5$. The influence of the aspect ratio b/a on the frequency is investigated in Figure 20. It was also observed that a decrement occurs for the results as the b/a increases.

Figure 21 reveals the effect of temperature ($\Delta T = 0$ K, 100 K, 300 K) on the transverse deflection with the thickness-to-side ratios $a/h = 4$. The deflection by the Voigt is minimum, the deformation increases as the temperature increases. Figures 22 and 23 depict the influence of temperature on the maximum non-dimensional deflection with a different non-homogeneity index $n = 0.5, 2, 5$ and a different aspect ratio $b/a = 1, 2, 4$. The results enhance as: 4.66%, 5.0%, 5.67 from $\Delta T = 0$ to $\Delta T = 500$ by the Voigt with the non-homogeneity index $n = 0.5, 2, 5$, respectively. The results enhance as: 5.0%, 4.94%, 4.92 from $\Delta T = 0$ to $\Delta T = 500$ by the Voigt with the aspect ratio $b/a = 1, 2, 4$, respectively.

6. CONCLUSIONS

For the appropriate thickness FGM plate, the transverse stretching deformation of the structure easily occurs during the actual deformation. However, most research on the response analyses neglect the effect of transverse stretching, which will lead to inaccurate calculation results. A quasi-3D hyperbolic shear deformation theory which considers the stretching effect are employed to predict the effect on the free vibration and static behavior. Five alternative micromechanical models (Voigt, Reuss, Tamura, LRVE, Hashin) are utilized to predict the valid material properties. The profile of an FGM plate is assumed by the P-FGM, S-FGM and E-FGM. Furthermore, the temperature effect of the micromechanical models on the fundamental frequency and transverse displacement for FGM plates have also been predicted.

The volume fraction of functionally graded materials has a significant impact on the mechanical behavior of the structure. Discussing different micromechanical models and FGM material distribution forms for predicting material properties can help researchers select appropriate theories for analysis, which is important for accurately estimating the structural characteristics of FGM structures. Hashin (LB) and Hashin (UB) are often used to provide more precise boundaries for the response domain of FGM structures. FGM structures are mainly designed suitable for high-temperature environments, therefore, the influence of temperature plays a crucial role in evaluating the performance of functionally graded materials. Discussing the influence of temperature on structural mechanical behavior under different micromechanical models is more conducive to promoting the structure to practical engineering applications.

Table 4. Comparison of non-dimensional frequency parameters for $Si_3N_4/SUS304$ FGM plates.

		Vigot		Reuss		Tamura		Huang and Shen[46]	
	mode	(1,1)	(1,2)	(1,1)	(1,2)	(1,1)	(1,2)	(1,1)	(1,2)
	n								
$T_l = 300$ K	0	12.082	28.430	12.082	28.430	12.082	28.430	12.495	29.131
$T_u = 300$ K	0.5	8.317	19.564	8.209	19.302	8.239	19.375	8.675	20.262
	1	7.287	17.127	7.211	16.937	7.232	16.990	7.555	17.649
	2	6.536	15.334	6.482	15.200	6.497	15.238	6.777	15.809
$T_l = 300$ K	0	12.021	28.286	12.021	28.286	12.021	28.286	12.397	29.083
$T_u = 300$ K	0.5	8.278	19.472	8.172	19.215	8.201	19.286	8.615	20.215
	1	7.253	17.050	7.180	16.865	7.200	16.916	7.474	17.607
	2	6.507	15.269	6.455	15.138	6.470	15.175	6.693	15.762
$T_l = 300$ K	0	11.912	28.031	11.912	28.031	11.912	28.031	11.984	28.504
$T_u = 600$ K	0.5	8.204	19.300	8.099	19.043	8.128	19.116	8.269	19.783
	1	7.189	16.900	7.114	16.711	7.136	16.765	7.171	17.213
	2	6.449	15.131	6.393	14.994	6.410	15.034	6.398	15.384

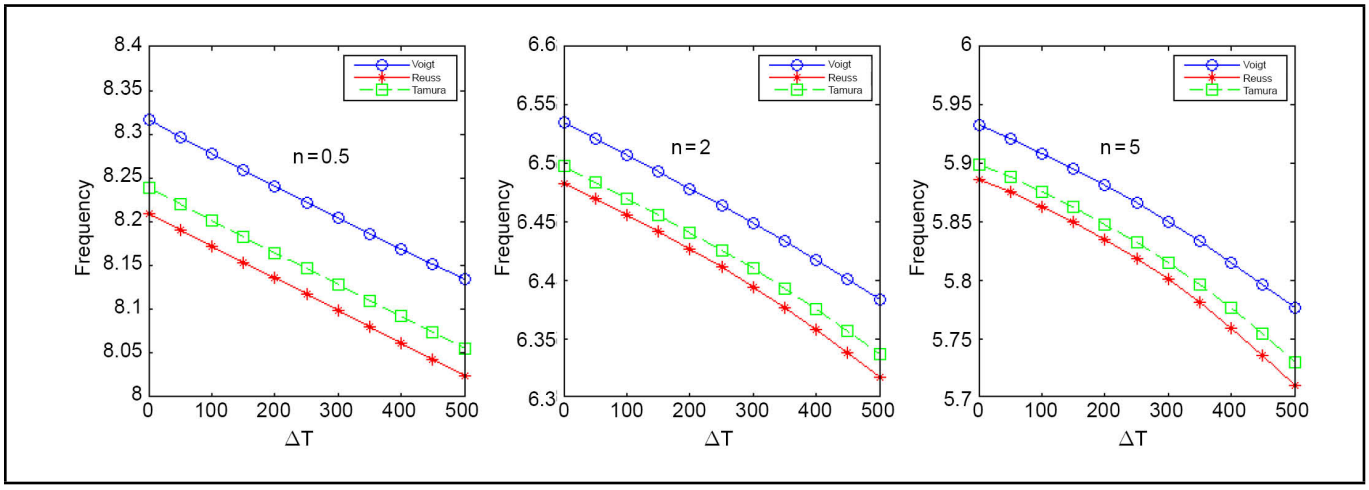

Figure 19. Non-dimensionalized fundamental frequencies with different non-homogeneity index n.

ACKNOWLEDGEMENTS

The authors gratefully acknowledge the support of the National Natural Science Foundation of China (12202038, and 12202069), the Guangdong Basic and Applied Basic Research Foundation (2021A1515110945), the Fundamental Research Funds for the Central Universities (FRF-TP-22-028A1), the China Postdoctoral Science Foundation (2022M720413, 2023T160047), R&D Program of Beijing Municipal Education Commission (KM202311232009).

DATA AVAILABILITY

Data used to support the findings of this study are included in the article.

REFERENCES

[1] Duc, N. D. and Tran, Q Q. Nonlinear postbuckling of imperfect eccentrically stiffened P-FGM double curved thin shallow shells on elastic foundations in thermal environments, *Composite Structures*, **106**, 590–600, (2013). https://doi.org/10.1016/j.compstruct.2013.07.010

[2] Farsani, S. R., Saadat, Z., Jafari-Talookolaei, R. A. et al. Free vibrational analysis of variable thickness plate made of functionally graded porous materials using internal supports in contact with bounded fluid, *Ocean Engineering*, **263**, 112335, (2022). https://doi.org/10.1016/j.oceaneng.2022.112335

[3] Chen, M. F., Wu, J. Z., Yin, C. H. et al. Three-dimensional vibration analysis of rotating pre-twisted variable thickness blades composed of spanwise graded functional materials, *Composite Structures*, **312**, 116836, (2023). https://doi.org/10.1016/j.compstruct.2023.116836

[4] Huang, Y. and Rong, H. W. Free Vibration of Axially Inhomogeneous Beams that are Made of Functionally Graded Materials, *International Journal Of Acoustics And Vibration*, **22** (1), 68–73, (2017). https://doi.org/10.20855/ijav.2017.22.1452

[5] Liu, S., Yu, T. T., Bui, T. Q. et al. Analysis of functionally graded plates by a simple locking-free quasi-3D hyperbolic plate isogeometric method, *Composites Part B-Engineering*, **120**, 182–196, (2017). https://doi.org/10.1016/j.compositesb.2017.03.061

[6] Jahangiri, M. and Bagheri, E. Effect of radially functionally graded materials on the primary resonances of large amplitude flexural vibration of in-extensional rotating shafts, *Engineering Structures*, **226**, 111362, (2021). https://doi.org/10.1016/j.engstruct.2020.111362

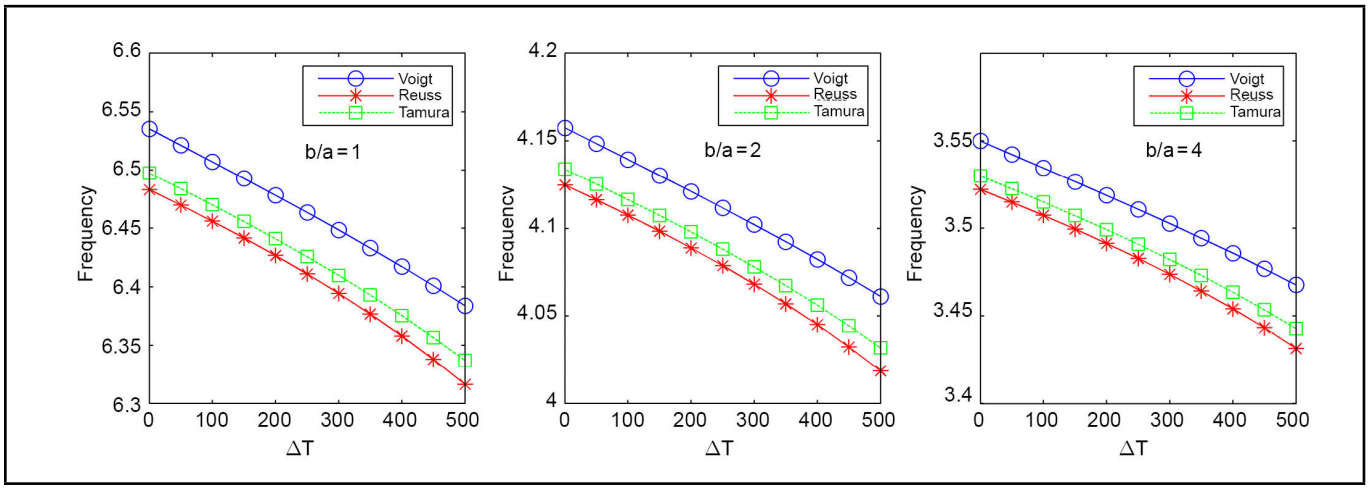

Figure 20. Non-dimensionalized fundamental frequencies with a different aspect ratio b/a.

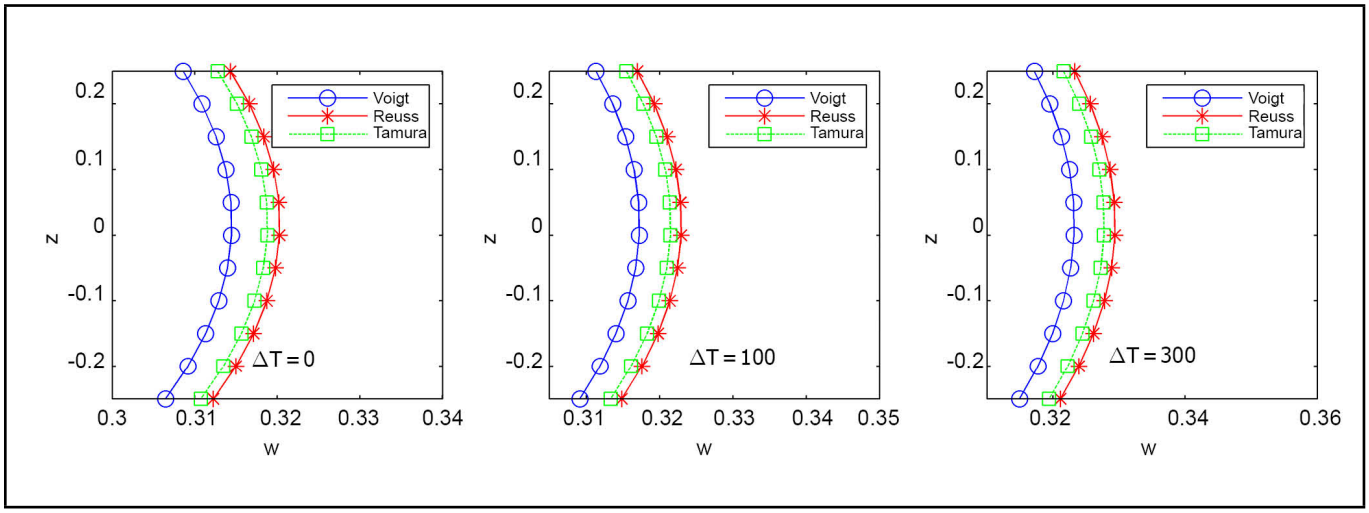

Figure 21. Distribution of displacement w through the thickness with different temperature.

[7] Zhou, L. L. Similitude analysis of free vibration of functionally graded material cylinders under thermal environment, *Mechanical Systems and Signal Processing*, **170**, 108821, (2022). https://doi.org/10.1016/j.ymssp.2022.108821

[8] Li, W., Hao, Y. X., Zhang, W. et al. Resonance response of clamped functionally graded cylindrical shells with initial imperfection in thermal environments, *Composite Structures*, **259**, 113245, (2021). https://doi.org/10.1016/j.compstruct.2020.113245

[9] Gasik, M. M. Micromechanical modelling of materials, *Computational Materials Science*, **13** (1–3), 42–55, (1998). https://doi.org/10.1016/S0927-0256(98)00044-5

[10] Rahman, S. and Chakraborty, A. A stochastic micromechanical model for elastic properties of functionally graded materials, *Mechanics of Materials*, **39**(6), 548–563, (2007). https://doi.org/ 10.1016/j.mechmat.2006.08.006

[11] Yin, H. M., Paulino, G. H., Buttlar, W. G. et al. Micromechanics-based thermoelastic model for functionally graded particulate materials with particle interactions, *Journal of the Mechanics and Physics of Solids*, **55** (1), 132–160, (2007). https://doi.org/10.1016/j.jmps.2006.05.002

[12] Muliana, A. H. A micromechanical model for predicting thermal properties and thermo-viscoelastic responses of functionally graded materials, *International Journal of Solids and Structures*, **46**, 1911–1924, (2009). https://doi.org/10.1016/j.ijsolstr.2009.01.008

[13] Akbarzadeh, A. H., Abedini, A., and Chen, Z. T. Effect of micromechanical models on structural responses of functionally graded plates, *Composite Structures*, **119**, 598–609, (2015). https://doi.org/10.1016/j.compstruct.2014.09.031

[14] Voigt, W. Über die beziehung zwischen den beiden elastizitätskonstanten isotroper körper, *Wied Ann Phys*, **38**, 573–587, (1889).

[15] Reuss, A. Berechnung der fliessgrenze von mischkristallen auf grund der plastizitsbedingung für einkristalle, *Zeitschrift für Angewandte Mathematik und Mechanik*, **9**, 49–58, (1929).

[16] Hashin, Z. The elastic moduli of heterogeneous materials, *ASME Journal of Applied Mechanics*, **29**, 143–150, (1962).

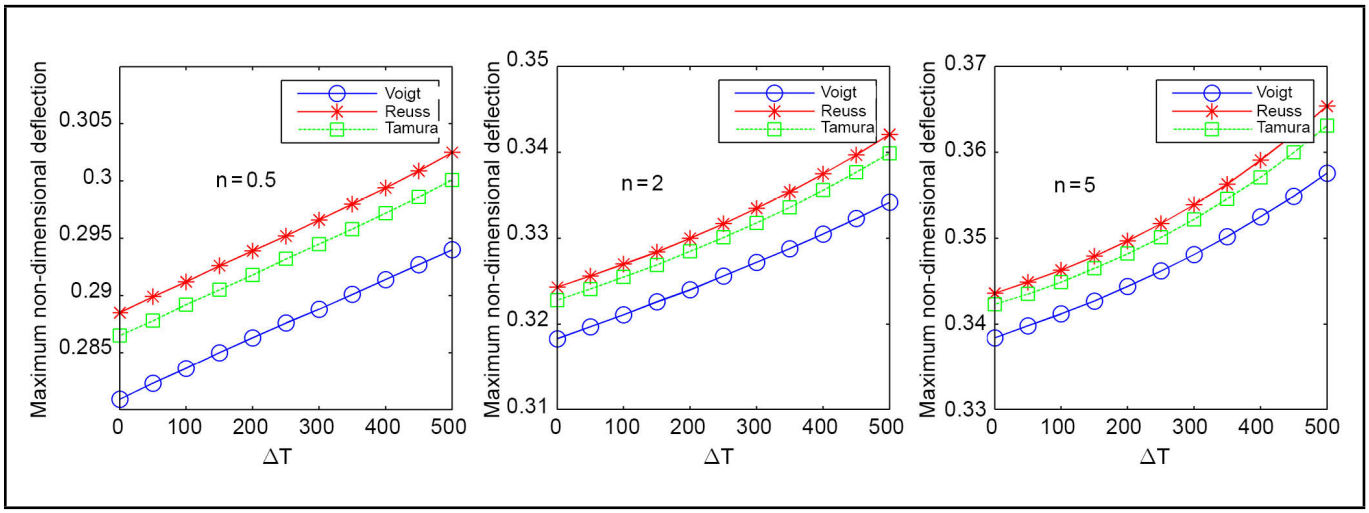

Figure 22. Maximum non-dimensional deflection with different non-homogeneity index n.

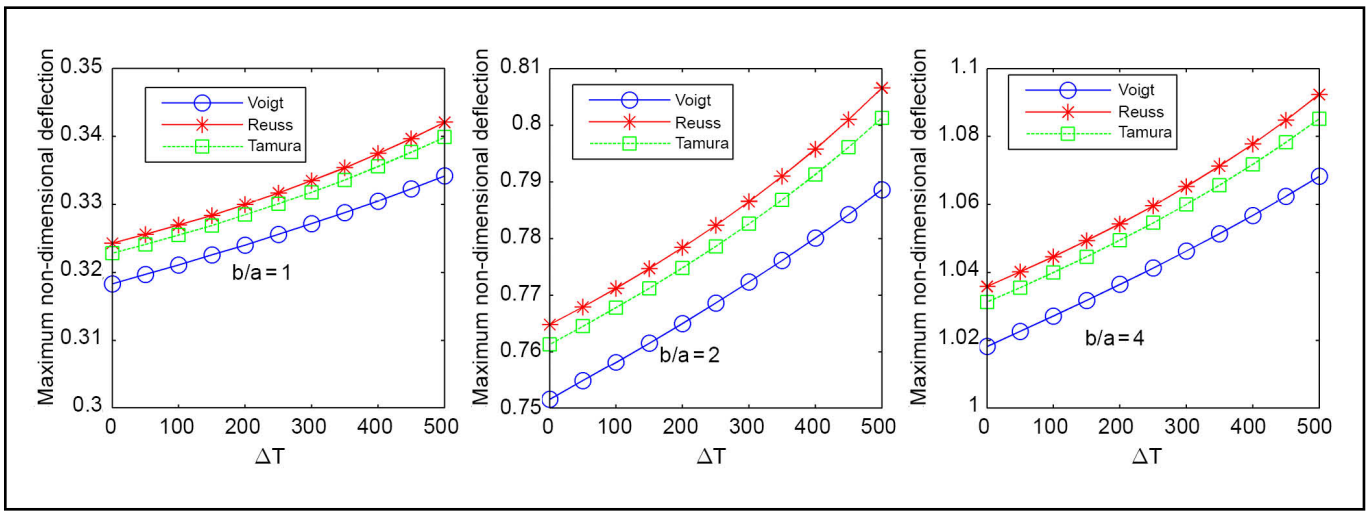

Figure 23. Maximum non-dimensional deflection with different aspect ratio b/a.

[17] Tamura, I., Tomota, Y., and Ozawa, M. Strength and ductility of Fe–Ni–C alloys composed of austenite and martensite with various strength, *Strength of Metals and Alloys*, **1**, 611–615, (1973).

[18] Gasik, M. and Lilius, K. Evaluation of properties of W–Cu functional gradient materials by micromechanical model, *Journal of Composite Materials*, **3**, 41–49, (1994).

[19] Shen, H. S. and Wang, Z. X. Assessment of Voigt and Mori-Tanaka models for vibration analysis of functionally graded plates, *Composite Structures*, **94**(7), 2197–2208, (2012). https://doi.org/10.1016/j.compstruct.2012.02.018

[20] Mindlin R. D. Influence of rotatory inertia and shear deformation on flexural motion of isotropic, elastic plates, *Journal of Applied Mechanics-Transactions of the Asme*, **18**, 31–38, (1951).

[21] Saeed, K., McIlhagger, A., Harkin-Jones, E. et al. Predication of the in-plane mechanical properties of continuous carbon fibre reinforced 3D printed polymer composites using classical laminated-plate theory, *Composite Structures*, **259**, 113226, (2021). https://doi.org/10.1016/j.compstruct.2020.113226

[22] Ramaswamy, S., Shariff, Z. A., Munaf, A. A. et al. Study on application of higher order lamination plate theory over various applications of natural fiber cross-ply composites, *Materials Today-Proceedings*, **60**, 822–826, (2022). https://doi.org/10.1016/j.matpr.2021.09.406

[23] Vinh, P. V. and Tounsi, A. Free vibration analysis of functionally graded doubly curved nanoshells using nonlocal first-order shear deformation theory with variable nonlocal parameters, *Thin-Walled Structures*, **174**, 109084, (2022). https://doi.org/10.1016/j.tws.2022.109084

[24] Najafipour, M. and Shariyat, M. A refined first-order shear deformation theory for large dynamic and static deflection investigations of abruptly/harmonically pressurized/blasted incompressible circular hyperelastic plates, *Ocean Engineering*, **289**, 116185, (2023).

[25] Reddy, J. N. A simple higher-order theory for laminated composite plates, *Journal of Applied Mechanics-Transactions of the Asme*, **51**, 745–752, (1984).

[26] Mantari, J. L., Oktem, A. S., and Soares, C. G. A new higher order shear deformation theory for sandwich and composite laminated plates, *Composites Part B-Engineering*, **43** (3), 1489–1499, (2012). https://doi.org/10.1016/j.compositesb.2011.07.017

[27] Van Do, V. N., Jeon, J. T., and Lee, C. H. Dynamic analysis of carbon nanotube reinforced composite plates by using Bezier extraction based isogeometric finite element combined with higher-order shear deformation theory, *Mechanics of Materials*, **142**, 103307, (2020). https://doi.org/10.1016/j.mechmat.2019.103307

[28] Mohammadi, H., Weeger, O., and Shojaee, M. Isogeometric technique for dynamic instability analysis of nanocomposite folded plates based on higher-order shear deformation theory, *Thin-Walled Structures*, **177**, 109467, (2022). https://doi.org/10.1016/j.tws.2022.109467

[29] Ebrahimi, F., Jafari, A. Thermo-Mechanical Vibration Analysis of Imperfect Inhomogeneous Beams Based on a Four-Variable Refined Shear Deformation Beam Theory Considering Neutral Surface Position, *International Journal Of Acoustics And Vibration*, **24** (3), 426–439, (2019). https://doi.org/10.20855/ijav.2019.24.31237

[30] Li, Q., Iu, V. P., and Kou, K. P. Three-dimensional vibration analysis of functionally graded material sandwich plates, *Journal of Sound and Vibration*, **311**(1–2), 498-515, (2008). https://doi.org/ 10.1016/j.jsv.2007.09.018

[31] Carrera, E., Brischetto, S., and Cinefra, M. Effects of thickness stretching in functionally graded plates and shells, *Composites Part B-Engineering*, **42** (2), 123–133, (2011). https://doi.org/10.1016/j.compositesb.2010.10.005

[32] Ferreira, A. J. M., Carrera, E., Cinefra, M. et al. Analysis of laminated shells by a sinusoidal shear deformation theory and radial basis functions collocation, accounting for through-the-thickness deformations, *Composites Part B-Engineering*, **42** (5), 1276–1284, (2011). https://doi.org/10.1016/j.compositesb.2011.01.031

[33] Mantari, J. L. A novel higher-order shear deformation theory with stretching effect for functionally graded plates, *Composites Part B-Engineering*, **45**, 268–281, (2013).

[34] Amabili, M. A non-linear higher-order thickness stretching and shear deformation theory for large-amplitude vibrations of laminated doubly curved shells, *International Journal of Non-Linear Mechanics*, **58**, 57–75, (2014). https://doi.org/10.1016/j.ijnonlinmec.2013.08.006

[35] Zhou, Y. H. and Kiani, Y. Vibrations of nonlocal polymer-GPL plates at nanoscale: application of a quasi- 3D plate model, *Mathematics*, **11**, 4109, (2023). https://doi.org/10.3390/math11194109

[36] Akbari, M., Sadighi, M., Eslami, M. R., and Kiani, Y. Axisymmetric free vibration analysis of functionally graded sandwich annular plates: a quasi-3d shear and normal deformable model, *International Journal of Structural Stability and Dynamics*, **23**, 2350086, (2023). https://doi.org/10.1142/S0219455423500864

[37] Jafari, P. and Kiani, Y. Free vibration of functionally graded graphene platelet reinforced plates: A quasi 3D shear and normal deformable plate model, *Composite Structures*, **275**, 114409, (2021). https://doi.org/10.1016/j.compstruct.2021.114409

[38] Jafari, P. and Kiani, Y. Analysis of arbitrary thick graphene platelet reinforced composite plates subjected to moving load using a shear and normal deformable plate model, *Materials Today Communications*, **31**, 103745, (2022). https://doi.org/10.1016/j.mtcomm.2022.103745

[39] Neves, A. M. A., Ferreira, A. J. M., Carrera, E. et al. A quasi-3D hyperbolic shear deformation theory for the static and free vibration analysis of functionally graded plates, *Composite Structures*, **94**, 1814–1825, (2012).

[40] Shariat, B. A. S. and Eslami, M. R. Buckling of thick functionally graded plates under mechanical and thermal loads, *Composite Structures*, **78**, 433–439, (2007).

[41] Li, J. H. and Liu, L. An efficient SBFEM-based approach for transient exterior vibro-acoustic analysis of power-law functionally graded shells, *Thin-Walled Structures*, **186**, 110652, (2023). https://doi.org/10.1016/j.tws.2023.110652

[42] Thang, P. T., Nguyen-Thoi, T., and Lee, J. Closed-form expression for nonlinear analysis of imperfect sigmoid-FGM plates with variable thickness resting on elastic medium, *Composite Structures*, **143**, 143–150, (2016). https://doi.org/10.1016/j.compstruct.2016.02.002

[43] Ali, M. I., Azam, M. S., Ranjan, V. et al. Free vibration of sigmoid functionally graded plates using the dynamic stiffness method and the Wittrick-Williams algorithm, *Computers & Structures*, **244**, 106424, (2021). https://doi.org/10.1016/j.compstruc.2020.106424

[44] Kashtalyan, M. and Menshykova, M. Three-dimensional elasticity solution for sandwich panels with a functionally graded core, *Composite Structures*, **87**, 36–43, (2009).

[45] Ezzin, H., Wang, B., and Qian, Z. H. Propagation behavior of ultrasonic Love waves in functionally graded piezoelectric-piezomagnetic materials with exponential variation, *Mechanics of Materials*, **148**, 103492, (2020). https://doi.org/10.1016/j.mechmat.2020.103492

[46] Huang, X. L. and Shen, H. S. Nonlinear vibration and dynamic response of functionally graded plates in thermal environments, *International Journal of Solids and Structures*, **41**, 240–2427, (2004).